ISSN 1819-7140, Russian Journal of Pacific Geology, 2016, Vol. 10, No. 3, pp. 218–229. © Pleiades Publishing, Ltd., 2016.
Original Russian Text © L.I. Polufuntikova, V.Yu. Fridovsky, 2016, published in Tikhookeanskaya Geologiya, 2016, Vol. 35, No. 3, pp. 75–87.

Lithological Features, Reconstruction of Redox Setting, and Composition of the Provenances of the Upper Triassic Kular–Nera Shale Belt

L. I. Polufuntikova[a, b] and V. Yu. Fridovsky[b, a]

[a]*Ammosov Northeastern Federal University, ul. Belinskogo 58, Yakutsk, 677000 Russia*
e-mail: pli07@list.ru
[b]*Institute of Geology of Diamond and Noble Metals, Siberian Division, Russian Academy of Sciences, pr. Lenina 39, Yakutsk, 677980 Russia*
e-mail: 710933@list.ru

Received September 7, 2015

Abstract—Comprehensive lithogeochemical analysis is carried out for Norian sediments from the central part of the Kular–Nera shale belt. The sediments are represented by alternation of sandstones and siltstones. Petrochemical typification shows that the sandstones are subdivided into graywacke, arkose, and subarenite, while the siltstones belong to shale. The Norian sediments were mainly deposited in an oxidizing environment of a well-aerated basin in the distal parts of the Verkhoyansk passive continental margin. They are characterized by a high sorting of sedimentary material. The correlation between the rock-forming elements and the wide range of $(La/Yb)_n$ ratios indicate that the sedimentation basin contained the disintegration products of both acid [$(La/Yb)_n$ = 10.52–27.26] and mafic [$(La/Yb]_n$ = 6.22–8.96)] rocks. The high values of the La/Sc and Th/Co ratios are typical of acid rocks. The low K_2O/Al_2O_3 values (0.16 ± 0.02) and high Zr/Sc ratio (10.1 ± 2.74) are typical of redeposited material. It is established that several provenances were involved in the formation of the Norian sediments in the central part of the Kular–Nera shale belt. Multicomponent clastics and well-sorted recycled material were supplied into the sedimentation basin.

Keywords: lithology, geochemistry, Upper Triassic, sandstones, siltstones, lithochemical modules, redox conditions, provenances, Kular–Nera shale belt, East Yakutia

DOI: 10.1134/S1819714016030052

INTRODUCTION

Upper Triassic terrigenous sequences are widespread east of the Siberian Platform. In the Verkhoyansk fold-and-thrust belt, they are represented by shallow-water coastal-marine and shelf sediments which pass into the slope and foot sediments of the continental margin of the Kular–Nera shale belt [13]. In recent years, the Triassic sediments of East Yakutia have been studied by many researchers [2, 3, 8–10, 14]. At the same time, some questions regarding their formation and subsequent changes, especially for the distal facies of the sedimentation basin, where shelf sediments are replaced by deep-water sediments, remain insufficiently studied. The Triassic sequences have attracted much attention not only because of the opportunity to decipher the Triassic sedimentation conditions and paleogeographical settings over the vast area of northeastern Russia, but also because of their association with numerous, frequently large, noble metal deposits [15–17, 27, 28].

In this work, we characterized the lithological features and the degree of postsedimentation transformations of the terrigenous sequences and also analyzed and deciphered the provenance composition and conditions of formation of the Late Triassic sediments of the Kular–Nera shale belt, which accumulated in the Oimyakon sedimentation basin. The basin was initiated on the eastern margin of the North Asian Craton in the Carboniferous during Middle Paleozoic rifting. A decrease of the basin in the late Triassic–Early Jurassic led to a change in the sedimentation conditions [11, 13].

In order to typify the sediments and to reconstruct their terrigenous provenances, the contents of rock-forming, trace, and rare-earth elements (Tables 1–3) were analyzed using modern classification diagrams and the most informative geochemical coefficients and modules. The average chemical compositions of the dacite, basalt, rhyolite, and sandstone were used during analysis [12]. A comparative characterization was performed for rocks of different stratigraphic levels and lithological types, including the Lower and Middle Norian (Upper Triassic) sandstones and siltstones and upper Norian siltstones.

Table 1. Contents of major rock-forming oxides (wt %) in the Norian deposits and values of petrochemical modules

	Lower substage (T_3n_1)						Middle substage (T_3n_2)								Upper substage (T_3n_3)			
	1	2	3	4	5	6	7	8	9	10	11	12	13	14	15	16	17	18
	mt-8	mt-9	er-1	er-2	k-6	ms-1	ap-1	ap-2	mt-z3	m-166	m-167	p-90	p-96	g-24	z-28	z-37	d-44	d-59
SiO_2	67.40	63.90	60.62	63.92	63.82	58.83	62.90	55.50	72.57	74.40	81.50	59.80	60.50	65.81	57.84	55.10	63.65	58.80
TiO_2	0.72	0.50	0.88	0.99	1.05	0.71	0.64	1.13	0.64	0.79	0.38	1.12	1.05	1.07	1.07	1.06	0.76	1.03
Al_2O_3	11.90	9.55	15.03	16.86	16.57	10.63	11.95	19.65	11.87	13.30	8.55	17.10	16.80	14.37	17.97	18.95	13.31	13.70
Fe_2O_3	1.34	0.48	6.87	5.90	6.83	7.71	4.38	2.61	5.59	2.10	2.88	7.90	6.63	6.84	8.54	1.34	8.47	1.80
FeO	3.97	4.07					0.25	5.78		1.04	0.77	0.32	1.22			6.79		6.75
MnO	0.09	6.00	0.08	0.03	0.03	0.33	0.37	0.07	0.04	0.01	0.03	0.08	0.07	0.04	0.03	0.08	0.13	0.08
MgO	1.64	1.96	2.52	2.33	2.51	3.45	0.21	2.93	1.37	0.55	0.31	0.95	1.31	2.28	2.71	3.38	3.18	2.51
CaO	2.09	3.13	1.50	0.56	0.39	6.17	8.01	1.13	0.82	0.75	0.27	1.04	1.31	1.28	0.42	1.65	1.61	2.18
K_2O	1.70	1.72	2.66	3.25	2.59	1.67	2.00	3.60	1.99	1.90	1.10	3.00	2.80	2.42	2.68	3.00	1.74	1.80
Na_2O	2.50	1.50	2.12	2.19	2.24	2.04	2.50	1.00	2.29	1.80	1.90	1.50	1.40	2.31	1.47	1.00	1.88	1.30
P_2O_5	0.19	0.16	0.24	0.20	0.20	0.19	0.11	0.18	0.13	0.10	0.08	0.21	0.20	0.18	0.25	0.16	0.17	0.18
SO_3	0.25	0.31					0.25	0.25		0.25	0.25	0.25	0.25			0.25		0.25
CO_2	3.52	5.41					5.32	0.84		0.20	0.26	0.92	1.32			1.94		5.10
L.O.I.	2.70	2.01					2.22	4.30		3.18	2.02	5.38	5.14			4.36		3.52
HM	0.27	0.32	0.38	0.37	0.38	0.33	0.28	0.53	0.25	0.23	0.15	0.44	0.43	0.34	0.48	0.51	0.36	0.40
AM	0.18	0.15	0.25	0.26	0.26	0.18	0.19	0.35	0.16	0.18	0.10	0.29	0.28	0.22	0.31	0.34	0.21	0.23
FM	0.10	0.10	0.15	0.13	0.15	0.19	0.08	0.20	0.10	0.05	0.05	0.15	0.15	0.14	0.19	0.21	0.18	0.19
TM	0.06	0.05	0.06	0.06	0.06	0.07	0.05	0.06	0.05	0.06	0.04	0.07	0.06	0.07	0.06	0.06	0.06	0.08
SM	0.21	0.16	0.14	0.13	0.14	0.19	0.21	0.05	0.19	0.14	0.22	0.09	0.08	0.16	0.08	0.05	0.14	0.09
PM	0.14	0.18	0.18	0.19	0.16	0.16	0.17	0.18	0.17	0.14	0.13	0.18	0.17	0.17	0.15	0.16	0.13	0.13
AM	1.47	0.87	0.80	0.68	0.87	1.22	1.25	0.28	1.15	0.95	1.73	0.50	0.50	0.96	0.55	0.33	1.08	0.72
NAM	0.35	0.34	0.32	0.32	0.29	0.35	0.38	0.23	0.36	0.28	0.35	0.26	0.25	0.33	0.23	0.21	0.27	0.23
IM	0.43	1.05	0.44	0.33	0.39	0.71	0.40	0.41	0.45	0.22	0.41	0.46	0.44	0.45	0.45	0.41	0.61	0.59
$K_2O + Na_2O$	4.20	3.22	4.78	5.44	4.83	3.71	4.50	4.60	4.27	3.70	3.00	4.50	4.20	4.73	4.15	4.00	3.62	3.10
$\log(SiO_2/Al_2O_3)$	0.75	0.83	0.61	0.58	0.59	0.74	0.72	0.45	0.79	0.75	0.98	0.54	0.56	0.66	0.51	0.46	0.68	0.63
$\log(Fe_2O_3/K_2O)$	−0.10	−0.55	0.41	0.26	0.42	0.66	0.34	−0.14	0.45	0.04	0.42	0.42	0.37	0.45	0.50	−0.35	0.69	0.00
K_2O/Al_2O_3	0.14	0.18	0.18	0.19	0.16	0.16	0.17	0.18	0.17	0.14	0.13	0.18	0.17	0.17	0.15	0.16	0.13	0.13

Analyses 1, 2, 7, 8, 10–13, 16, 18 were carried out at the GUGGP Yakutskgeologiya, Yakutsk, using the conventional "wet" chemical technique. Analyses 3–6, 9, 14, 15, 17 were performed at the Laboratory of Geochemical Methods of PGE Prospecting of GRF SVFU on an inductively coupled plasma emission spectrometer. Analyst Ya.B. Legostaeva. Samples: (1, 2, 7–10) sandstones, (3–6, 11–18) siltstones. Modules: (HM) hydrolyzate, (AM) alumina–silica; (FM) femic, (TM) titanium, (SM) sodium, (PM) potassium; (AM) alkaline; (IM) iron; (NAM) normalized alkalinity module.

Table 2. Contents of trace elements (ppm) and their main ratios in the Norian deposits

	Lower substage (T_3n_1)						Middle substage (T_3n_2)								Upper substage (T_3n_3)			
	mt-8	mt-9	er-1	er-2	k-6	ms-1	ap-1	ap-2	mt-z3	m-166	m-167	p-90	p-96	g-24	z-28	z-37	d-44	d-59
Ba	946.0	858.6	600.6	741.5	558.6	440.3	982.2	875.0	388.4	540.6	574.5	458.3	452.7	567.5	487.8	1110.0	308.5	921.4
Sr	338.5	324.8	218.0	161.5	131.7	257.3	555.0	492.5	130.4	313.4	316.1	456.2	420.0	242.9	151.2	524.1	131.4	469.1
Zn	332.0	339.4	87.8	76.6	105.3	94.1	439.5	427.4	61.9	370.8	346.1	406.5	390.2	87.6	101.7	521.1	102.5	477.1
V	41.3	42.1	114.7	133.9	182.3	101.0	77.2	76.0	111.8	84.6	90.2	154.8	148.9	132.1	219.3	72.7	100.6	61.4
Zr	54.1	51.5	232.5	264.0	251.4	223.7	60.4	60.7	116.6	72.6	79.8	61.4	62.1	214.7	264.2	60.5	125.5	50.3
Co	3.2	3.9	17.8	16.1	18.3	19.7	17.2	16.4	16.5	23.7	25.1	28.1	26.7	23.9	17.1	15.8	19.8	13.2
Cr	22.3	28.4	274.1	248.9	189.5	312.0	66.2	63.3	391.1	59.7	63.1	126.3	160.1	376.2	159.2	280.9	181.0	51.5
Cu	9.1	9.9	29.9	28.0	21.7	46.1	27.3	26.2	22.7	42.1	43.4	57.9	54.1	45.4	30.9	31.1	32.2	24.5
Li	110.4	113.6	374.3	360.9	596.4	435.5	332.7	323.1	316.7	103.5	107.5	251.0	239.5	472.7	1047.0	287.3	665.8	251.9
Ni	12.2	18.2	57.1	56.0	76.5	135.4	47.7	44.8	50.5	44.0	46.0	79.9	102.9	66.3	76.5	239.3	72.4	36.2
Sc	4.2	4.2	17.5	20.4	22.0	17.2	12.1	9.5	12.1	9.5	10.0	19.3	19.4	19.9	28.0	9.0	16.5	7.9
Be	2.3	2.4	2.1	2.4	2.3	1.7	2.4	2.4	1.5	2.0	2.1	1.6	1.5	2.0	2.3	2.7	1.6	2.6
Cd	1.0	1.0	2.1	2.0	2.2	2.2	2.0	2.0	1.7	1.9	2.0	2.5	2.3	2.1	2.5	2.2	2.4	1.8
Mo	2.0	2.1	2.0	3.0	1.7	2.3	1.6	1.5	2.0	1.3	1.2	1.4	1.6	3.7	2.7	3.3	1.9	1.7
Nb	8.4	10.0	31.2	36.5	35.2	30.0	13.2	12.6	23.3	11.7	12.4	16.5	16.4	34.0	36.4	12.7	24.3	10.8
Th	3.1	2.8	11.8	12.7	11.2	10.9	9.7	5.8	3.0	7.1	7.8	2.1	2.4	9.6	11.7	7.8	6.1	4.9
As	8.8	9.3	16.4	14.5	13.3	12.2	10.8	9.5	37.1	19.3	20.4	15.3	14.0	17.1	18.2	13.8	9.7	12.8
B	0.0	0.0	130.5	178.1	128.5	107.3	34.3	24.9	74.6	100.3	108.0	14.1	19.0	113.4	145.8	54.7	59.3	16.2
S	3983	4004	1162	231	555	4724	4870	4710	200	3093	3022	3153	3079	2651	1690	4663	286	4229
Ni/Co	3.8	4.7	3.2	3.5	4.2	6.9	2.8	2.7	3.1	1.9	1.8	2.8	3.9	2.8	4.5	15.2	3.7	2.8
Cr/V	0.5	0.7	2.4	1.9	1.0	3.1	0.9	0.8	3.5	0.7	0.7	0.8	1.1	2.9	0.7	3.9	1.8	0.8
V/(V+Ni)	0.8	0.7	0.7	0.7	0.7	0.4	0.6	0.6	0.7	0.7	0.7	0.7	0.6	0.7	0.7	0.2	0.6	0.6
Mo/Mn	0.0029	0.000	0.0031	0.0140	0.0026	0.0107	0.0006	0.0028	0.0032	0.0168	0.0052	0.0055	0.0006	0.0068	0.0057	0.0105	0.0027	0.0101

Analyses were performed at the Laboratory of Geochemical methods of PGE Prospecting of GRF SVFU on an inductively coupled plasma emission spectrometry. Analyst Ya.B. Legostaeva.

Table 3. Contents of rare-earth elements (ppm) and values of their main ratios in the Norian deposits

	Lower substage (T_3n_1)						Middle substage (T_3n_2)								Upper substage (T_3n_3)		
	mt-8	mt1-9	er-1	er-2	k-6	ms-1	ap-1	ap1-2	mt-z3	m-166	m-167	p-90	p-96	g-24	z-28	d-44	d-59
La	38.08	38.08	36.60	42.80	38.30	35.20	53.03	42.92	25.40	32.30	33.99	26.29	24.46	37.10	37.30	25.70	44.90
Ce	64.03	62.58	52.10	61.70	56.60	49.20	86.56	70.33	49.90	63.44	65.96	47.43	43.87	53.70	58.30	50.90	73.65
Pr	9.05	10.56	3.60	2.40	2.80	5.90	29.14	22.62	1.40	30.23	31.56	22.98	20.78	3.50	3.60	3.70	16.79
Nd	26.07	27.21	31.20	36.50	35.20	30.00	39.66	33.01	23.30	23.85	25.04	22.16	20.54	34.00	36.40	24.30	32.28
Sm	5.16	5.49	5.80	6.80	7.80	5.90	6.35	5.33	4.10	3.34	3.09	4.21	4.35	7.20	7.80	4.30	5.86
Eu	0.84	0.81	1.50	1.30	1.40	1.50	1.45	1.26	1.10	1.10	1.15	1.18	1.05	1.40	1.60	1.30	1.17
Gd	6.61	7.23	4.70	5.20	5.50	5.50	14.49	12.79	3.40	12.62	13.37	14.62	14.10	5.80	5.70	4.30	11.08
Dy	2.61	2.58	4.20	4.10	4.00	5.20	4.98	4.08	2.60	4.47	4.72	3.93	3.87	4.20	4.70	4.00	3.75
Ho	0.05	0.10	0.80	0.70	0.70	0.90	0.44	0.30	0.50	0.96	0.95	0.28	0.13	0.70	0.90	0.90	0.14
Er	n.d.	n.d.	1.50	1.90	1.90	1.70	n.d.	n.d.	0.90	4.21	4.41	5.10	6.20	1.70	1.90	1.10	n.d.
Yb	1.41	1.32	2.30	2.50	2.60	2.40	2.72	2.38	1.80	2.47	2.64	2.70	2.56	2.30	3.00	2.20	2.09
Lu	0.00	0.00	0.20	0.20	0.20	0.20	0.00	0.00	0.20	1.00	1.00	1.00	1.00	0.20	0.30	0.20	1.00
Y	11.93	11.12	24.20	25.10	24.60	27.70	24.16	18.35	17.70	16.19	17.46	16.06	15.32	24.20	27.70	22.80	16.48
Σ	166.0	167.0	169.0	191.0	182.0	171.0	262.0	212.0	132.0	194.0	205.0	168.0	158.0	176.0	189.0	146.0	214.0
Ce/Ce*	2.72	2.57	2.59	2.73	2.76	2.39	2.11	2.15	3.72	2.03	2.01	1.93	1.94	2.65	2.85	3.47	2.39
Gd_n/Yb_n	5.79	5.79	1.71	1.76	1.77	1.88	3.86	5.38	1.53	5.38	3.58	4.14	3.86	2.1	1.59	1.6	4.55
Eu/Eu*	0.52	0.52	0.87	0.69	0.68	0.81	0.33	0.38	0.91	0.49	0.49	0.39	0.41	0.67	0.74	0.93	0.38
La_n/Yb_n	27.26	27.26	11.5	12.5	10.73	10.52	12.67	15.42	9.98	11.48	8.13	6.22	5.74	11.71	8.96	8.28	16.14
LREE (L)	143.2	144.7	130.8	151.6	142.1	127.6	216.2	175.5	105.3	154.3	160.8	124.3	115.1	136.7	145.1	110.1	174.7
HREE (H)	10.7	11.2	13.7	14.5	14.9	15.8	22.6	19.6	9.4	25.7	27.1	27.6	27.9	14.9	16.5	12.7	18.1
L/H	13.42	12.89	9.54	10.44	9.53	8.09	9.55	8.98	11.25	6	5.93	4.5	4.13	9.21	8.82	8.68	9.67

Analyses were performed at the Laboratory of Geochemical Methods of PGE Prospecting of GRF SVFU. Analyst Ya.B. Legostaeva. REE contents were normalized after [34].

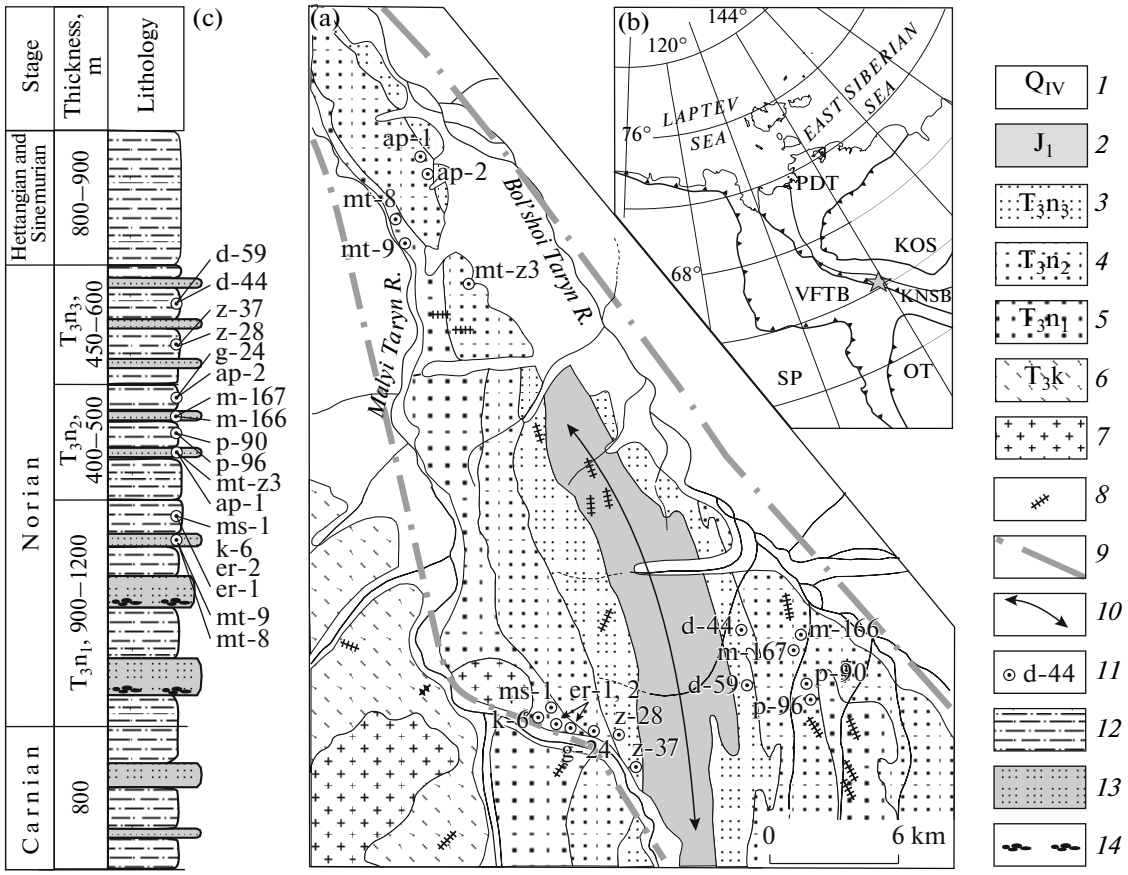

Fig. 1. Geological scheme of the Bol'shoi and Malyi Taryn interfluve (a) and its position in the review map (b) and stratigraphic column of the Upper Triassic and Lower Jurassic sediments (c).

(*1*–*6*) Sediments: (*1*) modern and Upper Quaternary alluvial deposits; (*2*) Lower Jurassic; (*3*–*6*) Late Triassic: (*3*) Upper Norian, (*4*) Middle Norian, (*5*) Lower Norian, (*6*) Carnian; (*7*) Early Cretaceous granitic massifs; (*8*) Late Jurassic dikes of diorite porphyrites and rhyolite porphyry; (*9*) branches of the Adycha–Taryn fault zone; (*10*) axis of the Malyi Taryn syncline; (*11*) sampling localities and numbers. Stratigraphic column: (*12*) siltstones, (*13*) sandstones, (*14*) conglomerate lenses.

Inset: (SP) Siberian platform, (VFTB) Verkhoyansk Fold-Thrust belt; (OT) Okhotsk Terrane; (KOS) Kolyma–Omolon Superterrane; (KNSB) Kular–Nera Shale Belt; (PDT) Polousnyi–Debin terrane.

GENERAL INFORMATION

The studies were carried out in the Taryn River basin (the right tributary of the Indigirka River). The Upper Triassic of the considered territory is represented by Carnian (T_3k) and Norian (T_3n) sediments [1] (Fig. 1). The Carnian sediments are dark gray to black bedded sitlstones with thin intercalations of reddish-gray fine-grained sandstones. The visible thickness is around 800 m.

The Norian sediments are the most widespread in the studied territory and are subdivided into three substages. The lower substage (T_3n_1) is represented by alternating siltstones and quartz–feldspathic and quartz sandstones with lenses of fine pebbly conglomerates. The lower substage sequences (900–1200 m thick) were mapped on the northwestern flank of the Bol'shoi and Malyi Taryn interfluve. The Middle Norian (T_3n_2) sediments 400–500 m thick are exposed as an S–N trending band in the interfluve of the main water streams and in the basins of the left tributaries of the Bol'shoi Taryn River. They are mainly represented by siltstones, with less abundant fine-grained sandstones. The Upper Norian is made up of 450–600 m thick siltstones with scarce sandstone intercalations. The Lower Jurassic sequence includes the sediments of the undivided Hettangian and Sinemurian stages (J_1g-s). They are recovered in the Malyi Taryn syncline and represented by siltstones and sandy siltstones. The sequence lies conformably and is 800–900 m thick.

PETROGRAPHY

Sandstones occur as gray and dark gray with a brownish tint; fine- to coarse-grained; mainly cross-lenticular; and fine- and coarse-bedded (more rarely massive) rocks. Transitional varieties (silty sandstones) show a spotted structure. The clastic material is represented by quartz, plagioclase, feldspar, fragments of volcanic rocks, muscovite, and biotite. Detrital miner-

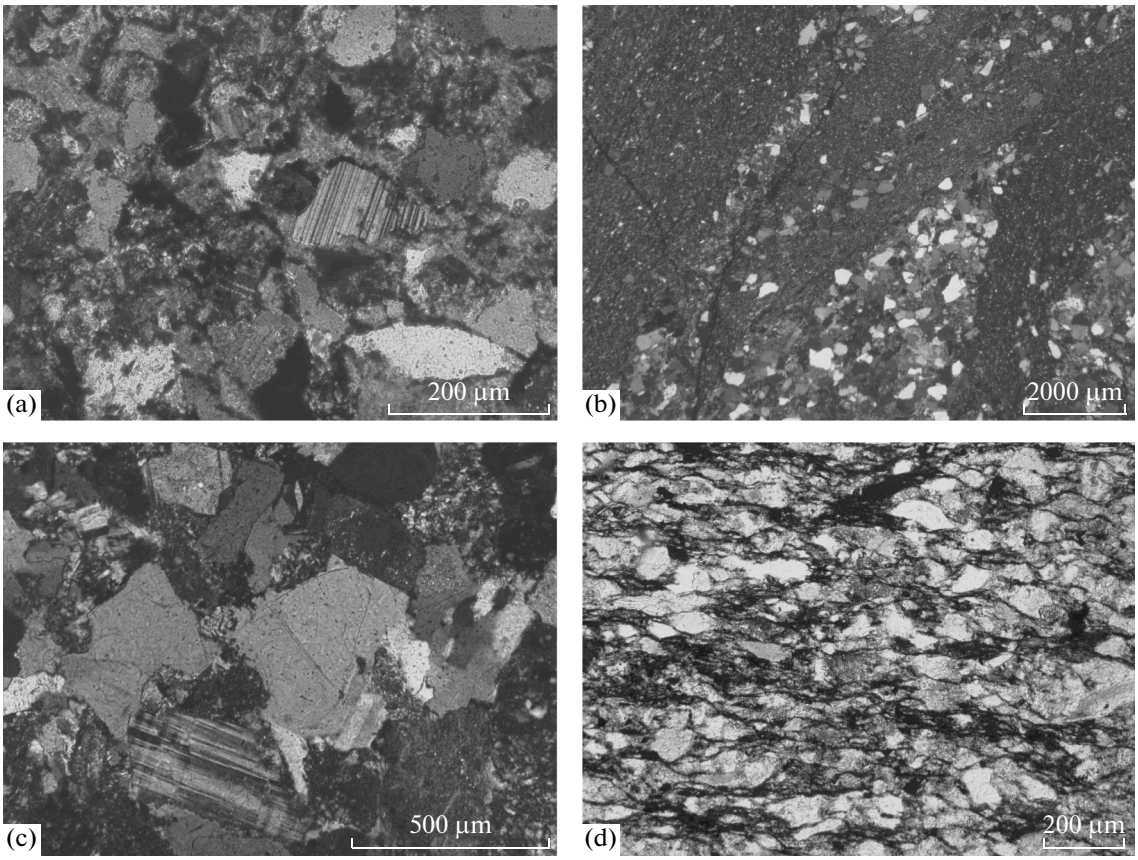

Fig. 2. Microimages of polished thin section from the Upper Triassic deposits of the central Kular–Nera shale belt.
(a) Fine-grained feldspar–quartz sandstones with mixed cement, T_3n_2; (b) fine cross-bedded siltstones, T_3n_3; (c) gravity corrosion structures, T_3n_1, with analyzer; (d) aggregate cleavage, without analyzer.

als are represented by equant to sharply elongated, semirounded to angular grains. The following types of cement are recognized in the sandstone: predominant contact basal, with less common filmy crustification, corrosion, and regeneration types. The cement is quartz–coaly–micaceous, chlorite–sericite–carbonate, and micaceous–chlorite–ferruginous in composition (Fig. 2a). In terms of the mineral composition, the sandstones are subdivided into quartz–feldspathic, polymictic, and calcareous varieties.

The siltstones are represented by dark gray; fine- to medium-grained; silty, psammitic–silty pelitic, and silty-pelitic rocks with lamination (Fig. 2b). The clastic material is represented by quartz, plagioclase, mica plates, and fragments of shales and volcanic rocks. The cement is basal, contact, pore-filling. It is quartz–sericite–chlorite and chlorite–clayeye–ferruginous in composition and contains carbonate and coaly material. Accessory minerals are apatite, rutile, and zircon.

Medium- to fine-pebbled conglomerates (pebble size 8–16 mm) form scarce dark gray spotted interbeds with psephitic texture. Pebbles composed of quartz, quartzite, volcanic rocks, hornfels, chert, and sandstones are cemented by the sericite–ferruginous matrix.

The sandstones were transformed under conditions of deep catagenesis–beginning of metagenesis [23, 24]. The compaction and chemical dissolution of the detrital grains led to the formation of the gravity corrosion texture and authigenic minerals (Fig. 2c). The detrital quartz is fringed by authigenic rims of regeneration quartz, while the interstitial space is filled with hypidiomorphic quartz–sericite aggregate showing a typical "checkerboard" extinction. Under stress conditions, the authigenic mica and chlorite form "beard-like" ingrowths into the quartz and feldspathic grains. More pervasive postsedimentation transformations are related to blastesis, which is manifested along the periphery of the detrital quartz, and to the initial stage of plagioclase albitization, accompanied by partial corrosion and regeneration of the grains.

The rocks in the fault influence zones experienced dynamometamorphism accompanied by textural–structural alterations. The siltstones and fine-grained sandstones in the regional fault zones record brittle–ductile and ductile shear zones of varying scale, which are associated with the tectonic flowing of the rocks

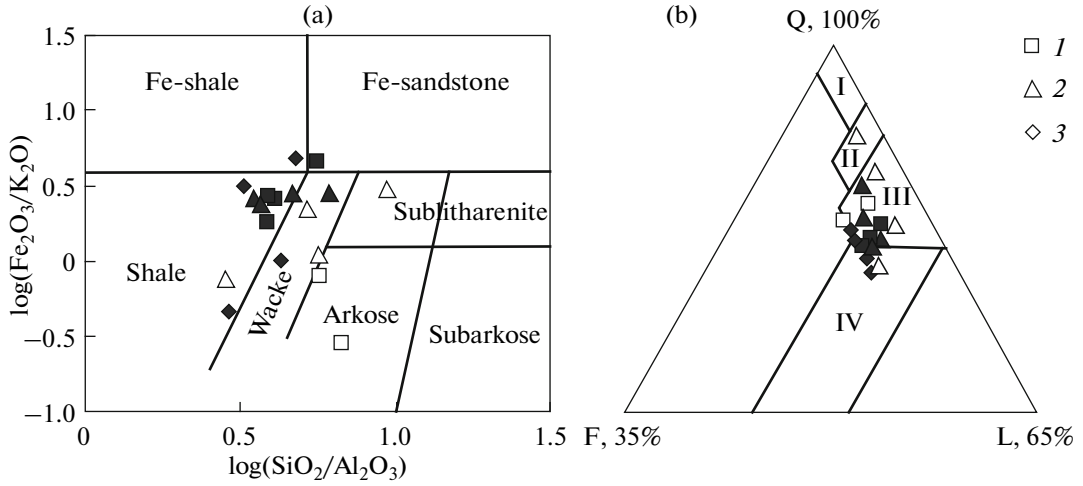

Fig. 3. Position of data points of the Upper Triassic sandstones and siltstones in the classification diagrams.
(a) Herron's diagram for sandstones and shales [30]; (b) diagram by Kossovskaya and Tuchkova [4] for sandstones.
Hereinafter: sediments of (*1*) lower substage, (*2*) middle substage, (*3*) upper substage. Filled symbols are siltstones, open symbols are sandstones. Coordinates: Q = SiO_2; F = Fe_2O_3 + FeO + MgO + MnO + TiO_2; L = Al_2O_3 + CaO + Na_2O + K_2O. Fields: (I) quartz sandstones, (II) oligomictic sandstones, (III) polymictic sandstones, (IV) volcaniclastic sandstones.

and formation of such indicative microtextures as aggregate-type and intergranular cleavage (Fig. 2d), deformation fibers, and pressure shadows, which in aggregate form a shear–cataclastic morphological type of flow textures [9].

The presence of the above-mentioned microtextural markers indicates that the deformation was a multistage and long-lasting process which resulted in the redistribution of diverse components in the fault influence zones. The brittle–ductile deformations operating at the initial stages caused the development of brecciation and aggregate-type cleavage. The ductile deformations were accompanied by the development of intergranular cleavage, porphyroblastic systems, and the wide distribution of oriented blastic and folded textures.

GEOCHEMISTRY

Examination of the chemical composition of the sediments (Table 1) allowed us to distinguish several features. The Al_2O_3 content in the sandstones is somewhat lower (average value of 11.19 ± 1.77) than that of the siltstones, which in addition show a wider range of variations from 10.63 to 19.65%, averaging 15.91 ± 2.59. The alkali contents are close in different lithological varieties and at different stratigraphic levels: the average K_2O content is 2.31 ± 0.45; Na_2O 1.83 ± 0.23; $K_2O + Na_2O = 4.14 \pm 0.43$. However, the rocks show a sufficiently wide scatter in Na_2O/K_2O ratio (from 0.28 to 1.73). The sandstones are dominated by sodium, while the siltstones by potassium. The sandstones (samples mt-8, mt-9, ap-1) are characterized by elevated CaO contents (from 2.09 to 8.01%). The contents of trace, including ore elements, show wide variations in different lithologies and at different stratigraphic levels. Normalization of the element contents in the Norian (Cn) rocks to their contents in sedimentary rocks (Ck) after Turekian and Wedepohl [5] revealed comparable contents of Ba, Sr, Co, Ni, Sc, and S ($0.94 < Cn/Ck < 1.16$); lower contents of V, Zr, Cu, Be, Cd, Th, and Mo ($0.31 < Cn/Ck < 0.83$); and extremely high (supraclarke) contents of Zn, Cr, Li, and As (Table 2). The sandstones differ in elevated Zn content (Cn/Ck = 3.96 ± 0.49), while the siltstones have elevated Li contents (Cn/Ck = 6.69 ± 3.55). The REE distribution (Table 3) shows no significant variations in the rocks from different stratigraphic levels and of different lithological types. The total REE + Y in the analyzed rocks varies from 158.23 to 222.24 ppm, averaging 190 ± 27.36. The REE pattern is characterized by a high LREE/HREE ratio (9.10 ± 2.43).

The petrochemical type of the rocks was determined using Herron's diagram [30] and the classification proposed by Kossovskaya and Tuchkova [4]. The former was used to classify the clastic rocks and to estimate the extent of preservation of Fe–Mg minerals, while the latter determines the sandstone associations. In Herron's diagram, the rocks are subdivided into petrographic varieties: the data points of the siltstones are confined to the shale field, while the sandstones are divided into wacke and arkose (Fig. 3a). In the diagram by Kossovskaya and Tuchkova (Fig. 3b), the data points of the rocks fall mainly in the field of polymictic sandstones and partially in the field of volcaniclastic rocks.

Lithochemical studies were carried out using the technique of Yudovich and Ketris [21, 22] based on the following modules: hydrolyzate HM = $(TiO_2 + Al_2O_3 + Fe_2O_3 + FeO + MnO)/SiO_2$, aluminum–silica ASM = Al_2O_3/SiO_2, iron IM = $(Fe_2O_3 + FeO + MnO)/TiO_2 + Al_2O_3$, alkaline AM = Na_2O/K_2O, normalized alkalinity NAM $Na_2O + K_2O/Al_2O_3$, and titanium TM = TiO_2/Al_2O_3. The sandstones have hydrolyzate module (HM) less than 0.3 and may be classified as clayey silicites and mesomictic and polymictic sandstones (Table 1). Based on the elevated content of detrital quartz and the low content of feldspar and clay minerals, they are highly mature rocks. In terms of all parameters (HM, TM, IM, FM, NKM, ASM, and AM), the siltstones are ascribed to normosiallites. Some siltstones may be ascribed to the pseudosiallite subtype—volcanosedimentary rocks. They differ in elevated contents of Mg (MgO > 3 wt %) at values of femic module within 0.18–0.21 (Table 1, an. ms-1; vs-37, d-44). In combination with the elevated K content (K_2O 3.0–3.6 wt %), this suggests the presence of both authigenic mica and sericite aggregates. Titanium module (TM) is an important geochemical characteristic of supergene processes, which is related to the dynamic sorting of material and the behavior of Ti-bearing minerals during sedimentation and further rock transformations [21]. It should be noted that the studied rocks are characterized by elevated (relative to the average chemical composition of the sedimentary rocks) Ti content (TiO_2 up to 1.13 wt %). According to the applied classification, the rocks in terms of TM values are normally titanium, but the Mesozoic sandy–clayey sediments have elevated TM = 0.06–0.08, which indicates the high dynamic sorting of the detrital component and the presence of volcanogenic material, possibly of mafic composition. As seen in the TiO_2–TM diagram (Fig. 4a), the Norian rocks are mainly restricted to the field of quartz sandstone, but some data points fall in the field overlap, which indicates the presence of mafic tuffs or tuffoids in the sampling.

In the HM–NAM diagram (Fig. 4b), the data points of the Norian (Upper Triassic) rocks define a negative correlation ($r = -0.79$) between the average compositions of the basalt, dacite, and sandstone. The different composition of the material delivered to the sedimentation basin is also observed in the F1–F2 diagram proposed by Bchatia and Crook [25] (Fig. 4c): the siltstones are characterized by quartz clastics, while the data points of the sandstones fall at the boundary between the intermediate and felsic rocks. The wide range of $(La/Yb)_n$ ratios indicates the presence of disintegration products of both felsic [$(La/Yb)_n$ = 10.52–27.26] and mafic [$(La/Yb)_n$ = 6.22–8.96] rocks [6]. In the La/Sc–Th/Co diagram [26], the data points of the Norian sandstones and siltstones fall mainly in the region of felsic rocks (Fig. 4d). Analysis of the diagrams presented in Fig. 4 shows that the main contributor to the Lower Norian rocks consisted of quartz-rich felsic rocks. The Middle and Upper Norian rocks are characterized by a wider diversity of terrigenous sources. Thus, the Norian sediments have a mixed composition and diverse genesis, which was possibly caused by the involvement of several provenances in their formation.

The average value of the Ce anomaly is Ce/Ce* = 1.04 ± 0.17 ($Ce/Ce^* = Ce_n/((La_n + Pr_n)/2)$), which is typical of sediments forming in a passive continental margin setting [7]. The localization of the data points in the diagrams SiO_2–K_2O/Na_2O [33] and $(K_2O + Na_2O)$–$(SiO_2/20)$–$(TiO_2 + Fe_2O_3 + MgO)$ [32] (Fig. 5) along the boundaries of the fields of different geodynamic settings points to unstable sedimentation conditions, which is typical of the distal parts of the passive continental margins.

Another important problem in the understanding the compositional specifics of the provenances is the examination of the rocks for the presence of redeposited material, which is characterized by the following features: K_2O/Al_2O_3 ratio less than 0.3 [26]; elevated contents of Th, Y, and Zr; and practically invariable value of Eu anomaly (Eu/Eu*), which shows no fractionation relative to other REE during recycling [6]. The average K_2O/Al_2O_3 ratio in the Norian silty sandstones is 0.16 ± 0.02, while the Zr/Sc ratio reaches sufficiently high values (10.1 ± 2.74) (Fig. 6), which is typical of fine aluminosiliciclastics formed by erosion of a mature continental crust. The Eu/Eu* ratio is on average 0.52 ± 0.2 (<0.9), but the values show sufficiently wide variations from 0.33 to 0.93, which indicates the input of diverse erosion products in the sedimentation basin.

The redox setting in the near-bottom waters of the sedimentation basin plays a significant role during the formation of sediments. The Mo/Mn, V/(V + Ni), V/Cr, and Ni/Co ratios (Fig. 7), as well as the total Mn content, may be used as geochemical indicators of the redox state. According to Kholodov [18, 19], Mn and Mo are accumulated at similar rates in the oxygen-bearing settings of well-aerated basins, but the solubility of Mo decreases in H_2S-rich settings, which leads to its accumulation in sediments owing to coprecipitation with sulfides, while Mn concentrations strongly decrease in anoxic environments. The average Mo/Mn ratio in the Triassic silty sandy rocks is 0.004, which indicates the accumulation of primary sediments in oxic environments. The V/(V + Ni) index varies from 0.23 to 0.77, which corresponds to values typical of oxic and moderately anoxic near-bottom waters [29]. Nickel and cobalt are intensely absorbed by manganese oxides from water masses in oxic environments (i.e., in oxidizing conditions) and, in contrast, are released in suboxic and anoxic environments (reducing settings). The Ni/Co values presented in Table 2 usually vary within 1.8–4.7, corresponding to the oxide zone of the near-bottom waters. The V/Cr

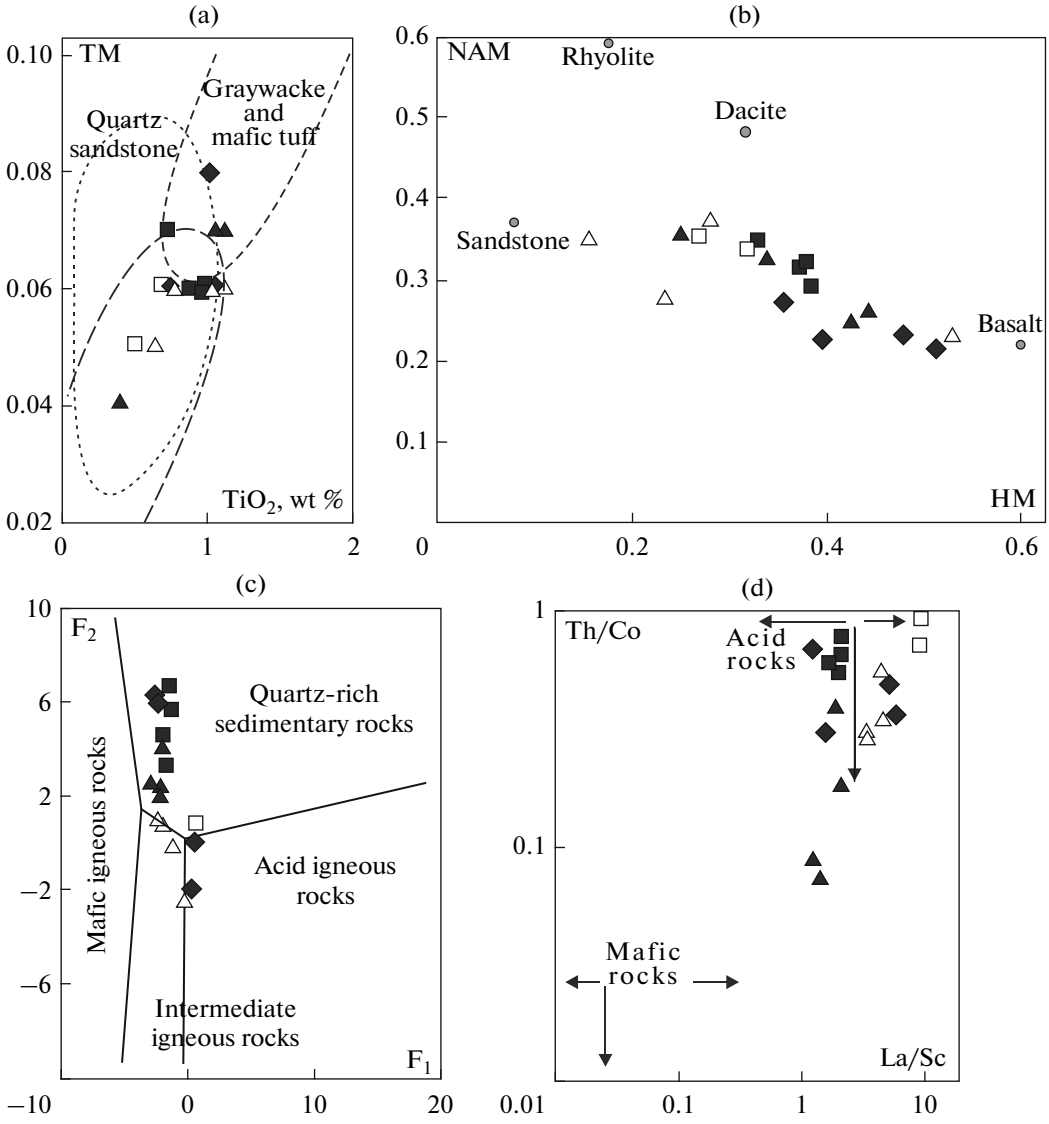

Fig. 4. Position of data points of the Upper Triassic sandstones and siltstones in the diagrams TiO_2–TM, HM–NAM [22]; F_1–F_2 [25], and La/Sc–Th/Co [26].

$F_1 = 0.303 + 0.0447SiO_2 - 0.972TiO_2 + 0.008Al_2O_3 - 0.267Fe_2O_3 + 0.208FeO - 3.082MnO + 0.14MgO + 0.195CaO + 0.719Na_2O - 0.032K_2O + 7.51P_2O_5$; $F_2 = 43.57 - 0.421SiO_2 + 1.988TiO_2 - 0.526Al_2O_3 - 0.551Fe_2O_3 - 1.61FeO + 2.72MnO + 0.881MgO - 0.907CaO - 0.177Na_2O - 1.84K_2O + 7.244P_2O_5$. Symbols are shown in Fig. 3.

ratio shows wide variations. According to Jones and Manning [31], the boundary between oxidizing and reducing near-bottom settings may be drawn at V/Cr = 2.0. The average V/Cr ratio in the studied rocks is 0.86 (V/Cr_{max} 1.85), which suggests that the studied sediments were mainly accumulated in oxic environments. It should be noted that the sandstones are characterized by elevated V/Cr = 1.2–1.9, while the siltstones have V/Cr ratio varying from 0.4 to 1.4. In general, this indicates an unstable setting and short-term changes of redox conditions in the near-bottom waters of the sedimentation basin [20] (Fig. 7). Thus, the Triassic sediments were formed in a well-aerated basin with clearly expressed redox settings.

CONCLUSIONS

The Upper Triassic sediments of the Kular–Nera shale belt are represented by the alternation of inequigranular siltstones and sandstones. In terms of the mineral composition, the sandstones are dominated by quartz varieties, while the siltstones have a mainly chlorite–smectite–hydromica composition. The postsedimentation transformations of the rocks

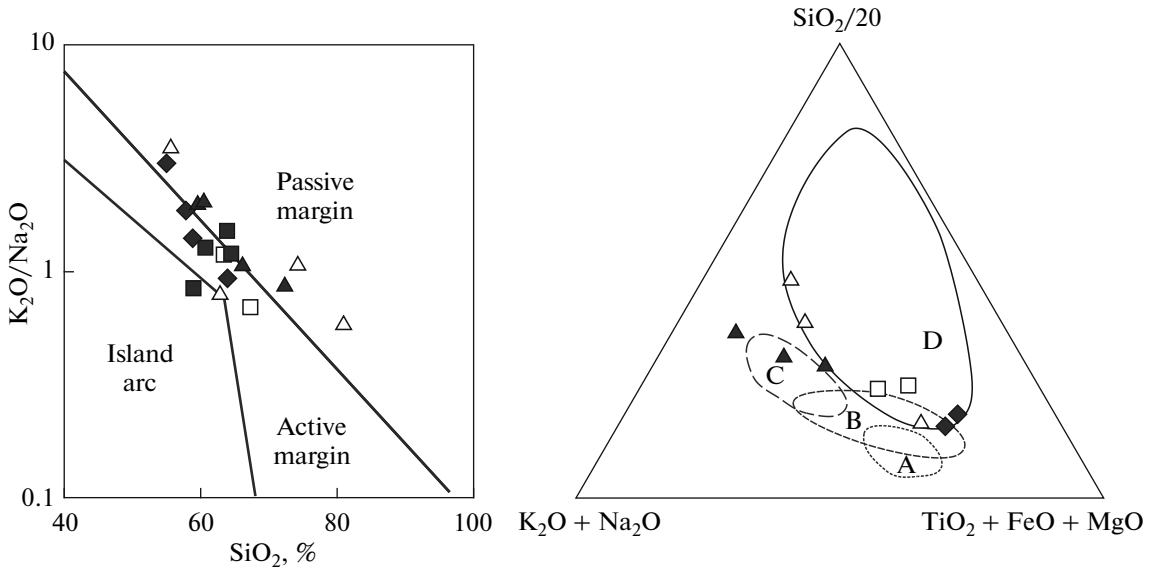

Fig. 5. Position of data points of the Norian rocks (Upper Triassic) in the SiO_2–K_2O/Na_2O diagram [33] and ($K_2O + Na_2O$)–($SiO_2/20$)–($TiO_2 + Fe_2O_3 + MgO$) [32]. Compositional fields: A, oceanic island arc; B, continental island arc; C, active continental margin; D, passive continental margin. Symbols are shown in Fig. 3.

reached deep catagenesis–beginning of metagenesis. The metagenetic transformations in the region are related to the P–T activation in response to a change of the geodynamic setting in the Late Jurassic. The dynamometamorphic transformations of the initial stage are mainly confined to the fault zones and marked by shear-cataclastic flow textures.

Our study showed that the Upper Triassic terrigenous sediments are subdivided into several petrochemical types: shale, wacke, arkose, and volcaniclastic varieties. According to the petrochemical classification, the Norian sandstones from the central part of the Kular–Nera shale belt are ascribed to the clayey silicites, while the siltstones are ascribed to the normosiallites. The elevated MgO and TiO_2 contents testify to the presence of alkaline mafic tuffoids of the pseudosiallite subtype. The studied rocks are characterized by the high sorting of sedimentary material. The Triassic sediments were formed mainly in oxidizing setting in a well-aerated basin in the distal parts of the Verkhoyansk passive continental margin.

The Upper Triassic sediments are characterized by a mixed composition and diverse genesis. The values of the $(La/Yb)_n$ ratio and the correlations between the hydralyzate module (HM) and total alkalinity module (TAM) indicate that the sedimentation basin contained disintegration products of both felsic and mafic rocks. The high La/Sc and Th/Co ratios are typical of felsic rocks. The low K_2O/Al_2O_3 ratios and high Zr/Sc are typical of redeposited material. Thus, several provenances supplied multicomponent clastics and well-sorted recycled material to the sedimentation basin. The disintegration products of felsic composition were presumably transported in the Oimyakon sedimentation basin from the southwest (Central Asian fold belt, Angara–Vitim batholith, and Aldan shield). Mafic clastic rocks were supplied by the Siberian trap province. The volcaniclastic material in the Late Triassic was derived from the southeast and east (Uda–Murgal island arc).

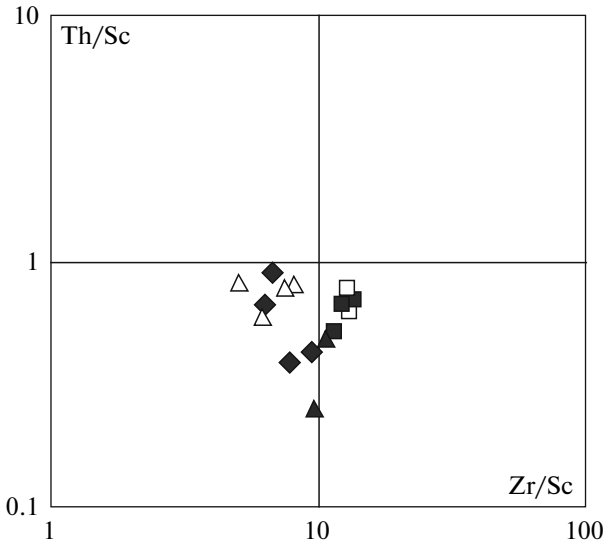

Fig. 6. Th/Sc–Zr/Sc diagram for the Norian (Upper Triassic) rocks. Symbols are shown in Fig. 3.

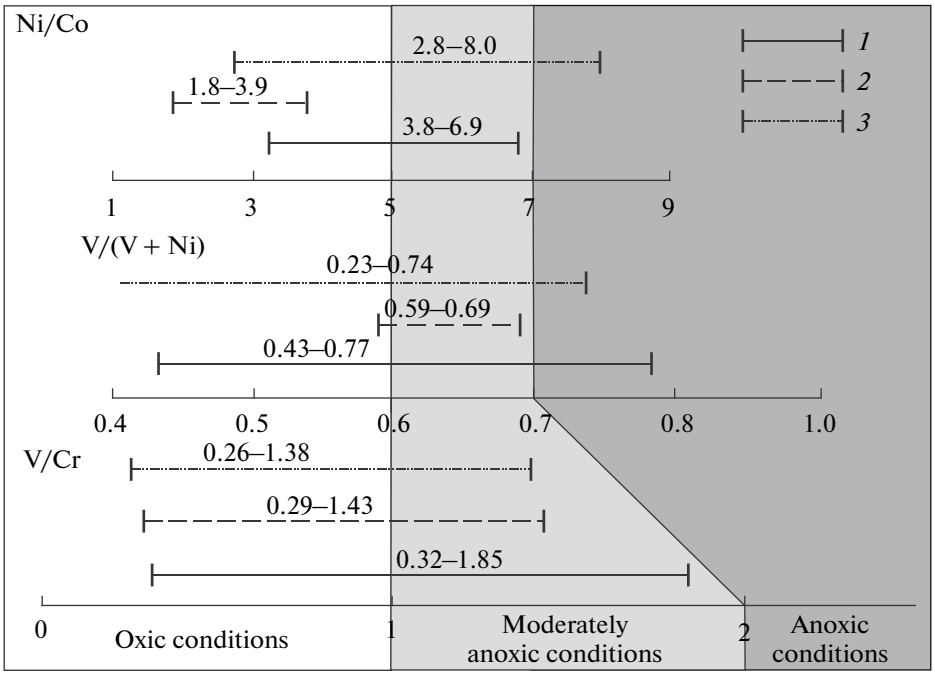

Fig. 7. Variations of geochemical indices Ni/Co, V/(V + Ni), and V/Cr at different states of the near-bottom water in the sedimentation basin.

(*1*) In the sediments of the lower substage; (*2*) sediments of the middle substage; (*3*) sediments of the upper substage.

ACKNOWLEDGMENTS

This work was supported by the Russian Science Foundation (project no. 141700465).

REFERENCES

1. V. S. Grinenko, V. B. Spektor, and V. S. Khan, *Geological Map of Yakutia. 1 : 500000. Verkhnyaya Indigirka Block. Sheets Q-53-A, B; Q-53-C, D; Q-54-A, B; Q-54-C, D, Q-55-A, B; Q-55-C, D,* Ed. by V. S. Grinenko, V. B. Spektor, and A. S. Urzov, (St. Petersburg Kartfabrika VSEGEI, St. Petersburg, 2000) [in Russian].
2. I. M. Gusev and V. V. Aristov, "Lithology and sedimentation conditions of Norian gold-bearing sequences in the central part of the Yana–Kolyma gold-bearing metallogenic province," Rudy Met., No. 1, 1–22 (2011).
3. M. M. Konstantinov, "Lithological–stratigraphic controle of gold-bearing deposits in sedimentary sequences," Regional. Geol. Metallogen., No. 36, 92–108 (2008).
4. A. G. Kossovskaya and M. I. Tuchkova, "On problem of mineralogical–petrochemical classification and genesis of sandy rocks," Litol. Polezn. Iskop., No. 2, 8–24 (1988).
5. *Brief Reference Book on Geochemistry. 2nd Edition* (Nedra, Moscow, 1977) [in Russian].
6. A. V. Maslov, *Sedimentary Rocks: Methods of Study and Interpretation of Obtained Data* (UGGU, Yekaterinburg, 2005) [in Russian].
7. A. V. Maslov, "Lithochemical appearance of sediments of the Vendian Asha Group, western slope of the South Urals," Litosfera, No. 1, 13–32 (2014).
8. L. M. Parfenov and A. M. Trushchelev, "Late Triassic Folding and olistostromes on the southwestern limb of the In'yali-Debin synclinorium, their tectonic position, and nature," Geol. Geofiz., No. 3, 7–20 (1983).
9. L. I. Polufuntikova and V. Yu. Fridovsky, "Microdeforamtion structures of the accretionary–collisional gold deposits: evidence from East Yakutia," Vestn. Severovost. Federal. Univ., **4** (1), 50–53 (2007).
10. A. V. Prokop'ev and A. V. Tronin, "Structural and sedimentation features of the junction zone between the Kular-Nera shale belt and In'yali-Debin synclinorium," Otechestvennaya Geol., No. 5, 44–48 (2004).
11. S. D. Sokolov, "Tectonics of Northeast Asia: an overview," Geotectonics, **44** (6), 493–509 (2010).
12. S. R. Taylor and S. M. McLennan, *The Continental Crust: Its Composition and Evolution* (Blackwell, London, 1985).
13. *Tectonics, Geodynamics, and Metallogeny of Sakha Republic Territory, Yakutia* (MAIK "Nauka/Interperiodika," Moscow, 2001) [in Russian].
14. M. I. Tuchkova, A. V. Prokop'ev, A. K. Khudolei, and V. E. Verzhbitskii, "Comparative analysis of conditions of Triassic sedimentation of Western Chukotka and southeastern flank of the Kular–Nera shale belt, Eastern Verkhoyansk Region," Uchen. Zap. Kazan. Univ. Estestven. Nauki **153** (4), 145–156 (2011).
15. V. Yu. Fridovsky, G. N. Gamyanin, and L. I. Polufuntikova, "Dora-Pil'sk ore field: structure, mineralogy, and geochemistry of the mineral formation," Rudy Met., No. 5, 7–21 (2012).
16. V. Yu. Fridovsky, G. N. Gamyanin, and L. I. Polufuntikova, "Gold–quartz and antimony mineralization in

the Maltan Deposit in Northeast Russia," Russ. J. Pac. Geol. **13** (8), 276–287 (2014).

17. V. Yu. Fridovskii, G. N. Gamyanin, and L. I. Polufuntikova, "Structures, mineralogy, and fluid regime of ore formation in the polygenetic Malo-Taryn gold field, Northeast Russia," Russ. J. Pac. Geol. **9** (4), 274–286 (2015).
18. V. N. Kholodov, "Evolution of provenances and sedimentary ore formation," Priroda, No. 1, 58–71 (1999).
19. V. N. Kholodov, "The role of H_2S-contaminated basins in sedimentary ore formation," Lithol. Mineral. Resour. **37** (5), 393–411 (2002).
20. V. Ernst, *Geochemcial Analysis of Facies* (Nedra, Leningrad, 1976) [in Russian].
21. Ya. E. Yudovich and V. N. Puchkov, "Geochemical diagnostics of deep-water sedimentary rocks," Geokhimiya, No. 3, 430–449 (1980).
22. Ya. E. Yudovich and M. P. Ketris, *Principles of Lithochemistry* (Nauka, St. Petersburg, 2000) [in Russian].
23. O. V. Yapaskurt, *Genetic Mineralogy and Stadial Analysis of Sedimentary Rock and Ore Formation* (ESLAN, Moscow, 2008) [in Russian].
24. O. V. Yapaskurt and S. E. Shikhanov, "Models of lithogenesis in the coeval Mesozoic North Siberian paleobasins of different types. Paper 2. Tectonic Mobile Belts," Byull. Mosk. O-va Ispyt. Prir., Otd. Geol. **4** (4), 58–73 (2009).
25. M. R. Bchatia and K. A. W. Crook, "Trace element characteristics of graywackes and tectonic setting discrimination of sedimentary basins," Contrib. Mineral Petrol. **92**, 181–193 (1986).
26. R. Cox, D. R. Lowe, and R. L. Cullers, "The influence of sediment recycling and basement composition on evolution of mudrock chemistry in the Southwestern United States," Geochim. Cosmochim. Acta **59**, 2919–2940 (1995).
27. R. J. Goldfarb, R. Taylor, G. Collins, N. A. Goryachev, and O. F. Orlandini, "Phanerozoic continental growth and gold metallogeny of Asia," Gondwana Res. **25** (1), 48–102 (2014).
28. N. A. Goryachev and F. Pirajno, "Gold deposit and gold metallogeny of Far East Russia," Ore Geol. Rev., No. 59, 123–151 (2014).
29. J. R. Hatch and J. S. Leventhal, "Relationship between inferred redox potential of the depositional environment and geochemistry of the Upper Pennsylvanian (Missourian) Stark Shale Member of the Dennis Limestone, Wabaunsee County, Kansas, USA," Chem. Geol. **99**, 65–82 (1992).
30. M. M. Herron, "Geochemical classification of terrigenous sands and shales from core or log data," J. Sediment. Petrol. **58**, 820–829 (1988).
31. B. Jones and D. A. C. Manning, "Composition of geochemical indices used for the interpretation of paleoredox conditions in ancient mudstones," Chem. Geol. **111**, 111–129 (1994).
32. S. B. Kroonenberg, "Effects of provenance, sorting and weathering on the geochemistry of fluvial sands from different tectonic and climatic environments," in *Proc. 29th Intern. Geol. Congress,* 1992 (VSP, Utrecht, 1994), part A, pp. 69–81.
33. B. P. Roser and R. J. Korsch, "Determination of tectonic setting of sandstone-mudstone suites using SiO_2 content and K_2O/Na_2O ratio," J. Geol. **94** (5), 635–650 (1986).
34. S.-S. Sun and W. F. McDonough, "Chemical and isotopic systematics of oceanic basalts: implications for mantle composition and processes," in *Magmatism in Ocean basins*, Ed. by A. D. Saunders and M. J. Norry, Geol. Soc. London, Spec. Publ. **42**, 313–345 (1989).

Recommended for publishing by N.A. Goryachev

Translated by M. Bogina